

Article

Photocatalytic Activity for Hydrogen Evolution of Heteroatom-Doped SrTiO₃ Prepared Using a Graphitic-Carbon Nitride Nanosheet

Keita Ikeue *, Yuta Yamamoto and Masashige Suzuki

Department of Applied Chemistry, Faculty of Engineering, Sanyo-Onoda City University, 1-1-1 Daigakudori, Sanyo-Onoda 756-0884, Yamaguchi, Japan; F118612@ed.socu.ac.jp (Y.Y.); F117604@ed.socu.ac.jp (M.S.)

* Correspondence: ikeue@rs.socu.ac.jp; Tel.: +81-836-88-4559

Received: 19 October 2019; Accepted: 3 January 2020; Published: 11 January 2020



Abstract: We developed a novel method to synthesize a visible-light-responsive photocatalyst from a composite of SrTiO₃ and a graphitic carbon nitride (g-C₃N₄) nanosheet. Heteroatoms were successfully doped into a lattice of SrTiO₃ by mild calcination of a composite that the g-C₃N₄ nanosheet adsorbed on to the SrTiO₃ surface. The absorption edge in the UV-Vis absorption spectrum of the doped sample was shifted to a longer wavelength region. The photocatalytic activity of the doped sample under UV light irradiation was higher than those of both pristine SrTiO₃ and the g-C₃N₄ nanosheet, suggesting that the photocatalytic property of SrTiO₃ was enhanced by doping. The doped sample showed photocatalytic activity under visible light irradiation (>420 nm), which was enhanced by Pt loading.

Keywords: photocatalyst; hydrogen evolution; visible light; SrTiO₃; g-carbon nitride nanosheet

1. Introduction

Hydrogen production by photocatalytic solar water splitting has received much attention as the next generation clean energy source because CO₂ emissions are minimal during electric power generation. Over the past few decades, a number of photocatalysts have been reported to achieve one-step overall water-splitting UV irradiation under visible light irradiation [1–10]. SrTiO₃ and TiO₂ have been widely used for water splitting photocatalysis under UV irradiation because of their non-toxicity and low cost [11–15]. However, these photocatalysts cannot operate under visible light irradiation because of their wide band gap. Many researchers have therefore developed visible-light-driven photocatalysts by band modification [16–20].

Doping, which includes replacing the host material with a foreign element at a crystal lattice point, is widely used to prepare visible-light-driven photocatalysts. Kudo et al. reported that co-doping of Cr³⁺-Ta⁵⁺ and Cr³⁺-Sb⁵⁺, and doping of Rh cations were effective, with doped SrTiO₃ showing high photocatalytic activity for H₂ evolution under visible light irradiation in the presence of a sacrificial agent [16,17]. The donor level was formed between the conduction band and the valence band. The transition from the donor level to the conduction bands of SrTiO₃ and TiO₂ responds to visible light absorption. For other band-modification methods in the oxide-based photocatalyst, sulfurization and nitridation have also been suggested. These processes were carried out by high-temperature calcination of an oxide-based photocatalyst in the flowing of H₂S and NH₃. The new bands based on S3p and/or N2p orbitals formed above O2p valence bands and led to a decrease in the band gap. Ohno et al. reported TiO_{1-x}S_x prepared by calcination of TiO₂ in the flowing of H₂S showed photocatalytic activity under visible light irradiation [18]. Domen et al., have reported on oxynitride- and oxysulfide-based photocatalysts for water splitting such as TaON, ATaO₂N (A = Ca, Sr, Ba),

(Ga_{1-x}Zn_x)(N_{1-x}O_x) solid solution and Ln₂Ti₂S₂O₅ (Ln = Pr, Nd, Sm, Gd, Tb, Dy, Ho and Er) [21–23]. In particular, an Rh_{2-y}Cr_yO₃-loaded (Ga_{1-x}Zn_x)(N_{1-x}O_x) solid solution synthesized by nitriding a mixture Ga₂O₃ and ZnO has been shown to achieve overall water splitting under visible light irradiation without noticeable degradation. The quantum efficiency of this photocatalyst for overall water splitting reached ca. 2.5% at 420–440 nm. However, doping and sulfurization/nitridation require high-temperature calcination and the use of toxic reactants, respectively. From the perspectives of energy consumption suppression and reducing environmental load, the development of a more environmentally friendly process is required.

In the present study, we investigated facile doping under mild conditions in order to obtain a visible-light-driven photocatalyst. Graphitic C₃N₄ (g-C₃N₄) nanosheets were used as a doping agent. The bulk g-C₃N₄, an organic, metal-free polymeric, layered semiconductor has recently attracted attention as a visible-light-responsive photocatalyst [9,24–28], and its photocatalytic property was first reported by Wang et al. [29]. Moreover, the composite photocatalysts using g-C₃N₄ were reported and show high photocatalytic activity [30–33]. The layered g-C₃N₄ can be exfoliated into 2D thinner nanosheets. Although many investigations on the photocatalysis using bulk g-C₃N₄ have been carried out, there are few studies using g-C₃N₄ nanosheets. Therefore, we focused on the synthesis of a photocatalyst using g-C₃N₄ nanosheets. The 2D g-C₃N₄ nanosheet will strongly interact with other oxide-based semiconductor surfaces due to its high surface energy. By using a strong interaction of 2D g-C₃N₄, doping was carried out by the calcination of g-C₃N₄ nanosheet-adsorbed SrTiO₃ nanoparticles in a nitrogen atmosphere. We optimized the amount of dopant by changing the volume of g-C₃N₄ nanosheet dispersion in the adsorption process. The photocatalytic hydrogen evolution in the presence of a sacrificial agent under UV and visible-light irradiation was studied. Moreover, we investigated the effect of co-catalyst loading on the photocatalytic activity under visible light irradiation.

2. Materials and Methods

2.1. Chemicals and Materials

Urea (99%), HNO₃ (70%), and HCl (37%) were purchased from FUJIFILM Wako Pure Chemical Co. Ltd. (Osaka, Japan). These chemicals were used without purification. SrTiO₃ nanoparticles were supplied by Toda Kogyo Co., Ltd., and calcined at 600 °C for 2 h before use.

2.2. Synthesis of Photocatalyst

A carbon nitride nanosheet was prepared following a method given in a previous study [34]. Urea was calcined at 600 °C in a crucible with a cover (heating rate: 5 °C/min) in order to obtain the bulk g-C₃N₄. The bulk C₃N₄ powder was washed with 0.1 M HNO₃ and distilled water, followed by drying at 70 °C for 12 h. The powder was dispersed into a 15% HCl aqueous solution (150 mL). The resulting suspension was sonicated for 1 h and was then magnetically stirred for 24 h. The suspension was transferred to Teflon-lined stainless steel autoclaves and heated to 110 °C for 5 h. The obtained suspension was pump filtrated and washed at least five times to remove HCl and agglomerate the C₃N₄. To achieve g-C₃N₄ nanosheet dispersion, the wet product was dispersed into 100 mL distilled water.

The calcined SrTiO₃ (0.3 g) was dispersed into 100 mL distilled water, followed by sonification for 10 min. The g-C₃N₄ nanosheet dispersion was dropped into the SrTiO₃ dispersion under vigorous stirring. The amount of the dropped g-C₃N₄ nanosheet dispersion was varied in the range of 10 to 30 mL. The resulting suspension was stirred at room temperature for 1 h, and left without stirring for 3 h. The obtained sedimentation was centrifugated and dried at 110 °C overnight. The resulting powder was calcined at 600 °C for 5 h in flowing N₂. The doped sample was abbreviated as SrTiO₃-D_x (x is volume of added g-C₃N₄ nanosheet dispersion).

2.3. Characterization

The crystal structures of the samples were determined using an X-ray diffraction (XRD) diffractometer (Rigaku, SmartLab, Tokyo, Japan) with monochromated Cu K_{α} radiation (40 kV, 30 mA). X-ray fluorescence (XRF; Horiba, XGT-7200, Tokyo, Japan) analysis was used to obtain the chemical composition of the samples. For the samples, the microstructures were observed and local elemental analysis was conducted using field emission scanning electron microscopy (FE-SEM) with energy-dispersive X-ray analysis (EDX, Hitachi S-4800, Tokyo, Japan). Diffuse reflectance absorption spectra were recorded using a UV-Vis spectrometer (Shimadzu, UV-3100PC, Kyoto, Japan) to determine the optical band gap energy.

2.4. Photocatalytic Reaction

The photocatalytic reaction was conducted in an external-irradiation quartz cell connected to a closed gas-circulating system. The photocatalyst (0.1 g) was suspended in 50% methanol aqueous solution (150 mL) in the cell. The rate of H_2 evolution was determined via gas chromatography (Shimadzu GC-8A, TCD, Ar carrier, MS-5A) under irradiation from a 500 W Xe lamp (light density at 420 nm: 0.23 W/cm^2 , illuminated area: 78.5 cm^2 , distance between light source and cell: 10 cm). The light wavelength was controlled using a cut-off filter (Sigma Koki, Saitama, Japan). Additionally, the photocatalytic reaction was carried out after Pt photodeposition.

3. Results and Discussion

3.1. Characterization of Doped $SrTiO_3$

A nanosheet will have an unstable surface compared to bulk material because of its high surface energy. Therefore, a g- C_3N_4 nanosheet will strongly adsorb $SrTiO_3$ nanoparticles to form the precursor material for a doped sample. The doped sample can be synthesized by a solid state reaction between the g- C_3N_4 nanosheet and $SrTiO_3$ owing to strong interaction. To optimize the amount of adsorbed g- C_3N_4 nanosheet in the precursor material, we synthesized the doped sample by changing the volume of g- C_3N_4 nanosheet dispersion. The crystal structures of the as-prepared samples were examined via XRD. Figure 1 shows the XRD patterns of pristine $SrTiO_3$, g- C_3N_4 nanosheet, and the doped samples. The XRD pattern of the pure g- C_3N_4 nanosheet exhibited two diffraction peaks at 13.2° and 27.6° , which corresponded to the (100) and (002) diffraction planes, respectively [25,29,35]. These were attributed to the characteristic in-plane and inter-planar stacking peaks of the aromatic system in graphite-like carbon nitride, respectively [29]. The pristine $SrTiO_3$ exhibits five distinct peaks at 22.66° , 32.27° , 39.79° , 46.28° , 52.11° , and 57.53° , which can be attributed to the (100), (110), (111), (200), (210), and (211) crystal planes, respectively. The doped samples were not observed as having the peaks owing to the g- C_3N_4 ; only the peaks ascribed to $SrTiO_3$. It is suggested that this sample was not a simple composite of g- C_3N_4 and $SrTiO_3$ nanoparticles. However, the diffraction peaks at 32.34° for the (110) planes of the doped samples ($SrTiO_3$ -D15) exhibited a slightly higher shift than that of pristine $SrTiO_3$ (32.27°), which indicated that nitrogen or carbon was doped into $SrTiO_3$, resulting in lattice distortion. The shift was also observed on other doped samples (Table S1).

The morphologies of the doped samples were examined via FE-SEM (Figure 2). As shown in Figure 2a, uniform spherical nanoparticles with grain sizes of approximately 30 nm could be observed. The g- C_3N_4 nanosheet particles (Figure 2b) had a thin lamellar shape and obvious particle aggregation was observed. Nanosheet aggregation may occur during the drying process. In the FE-SEM image (Figure 2c) of the calcination product from the $SrTiO_3$ /g- C_3N_4 composite, g- C_3N_4 nanosheet particles were not observed, which made it difficult to differentiate pristine $SrTiO_3$ from the doped sample. From the energy dispersed X-ray spectroscopy (EDX) analysis results for pristine $SrTiO_3$ and $SrTiO_3$ -D15 (Figure 3), it can be seen that the content of the C element in the doped sample is notably higher than that of pristine $SrTiO_3$. In addition, the presence of the N element was observed in the doped sample, indicating that C and N were successfully doped into the lattice of $SrTiO_3$.

We attempted to perform an X-ray photoelectron spectroscopy (XPS) analysis of the doped samples to elucidate the chemical state of C and/or N. However, we could not sufficiently obtain the XPS spectra because of low concentration.

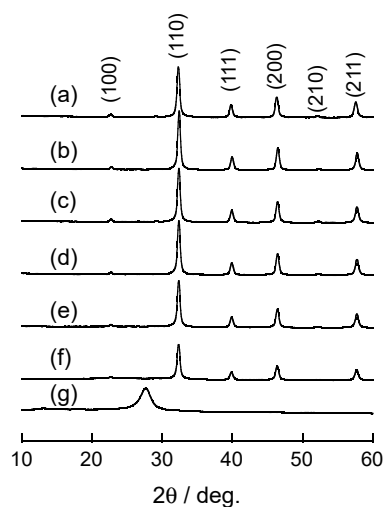


Figure 1. X-ray diffraction (XRD) patterns of (a) pristine SrTiO₃, (b) SrTiO₃-D10, (c) SrTiO₃-D15, (d) SrTiO₃-D20, (e) SrTiO₃-D25, (f) SrTiO₃-D30, and (g) C₃N₄.

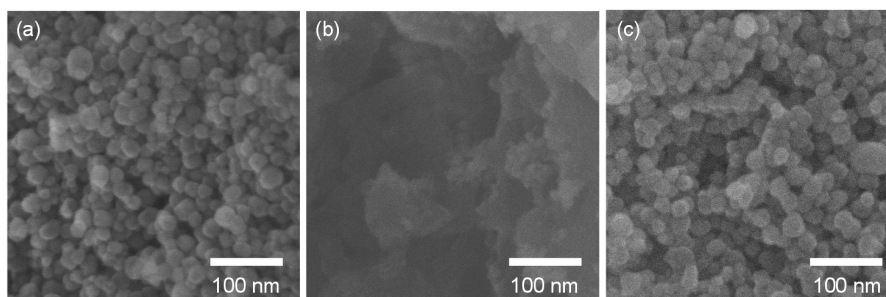


Figure 2. Scanning electron microscopy (SEM) images of (a) pristine SrTiO₃, (b) pristine g-C₃N₄, and (c) SrTiO₃-D15.

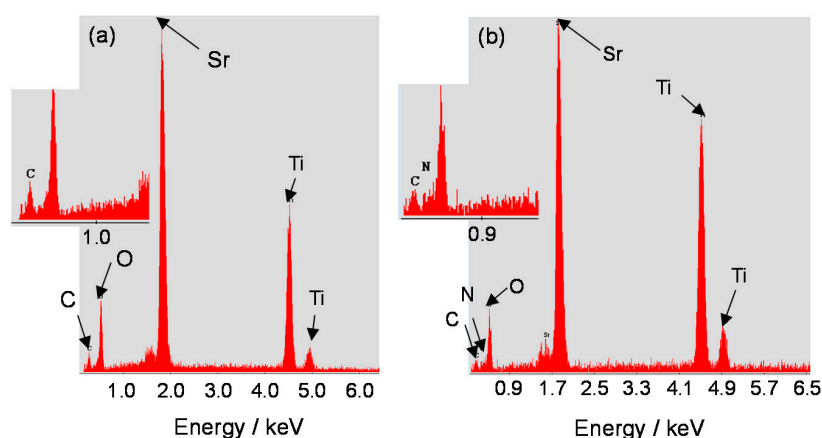


Figure 3. Energy-dispersive X-ray (EDX) spectra of (a) pristine SrTiO₃ and (b) SrTiO₃-D15.

The diffuse reflectance absorption spectra were used to study the optical properties of the doped samples. Figure 4 shows the diffuse reflectance UV-Vis absorption spectra of the doped samples. The doped samples exhibited a longer light absorption edge compared to pristine SrTiO₃, indicating that C or N doping was an efficient alternative for expanding light absorption by SrTiO₃. Moreover,

an obvious red shift was observed in the absorption edge of the doped samples. We also observed color change of samples from white to light yellow after doping (Figure S1). Figure 4b shows the Tauc plots obtained from the UV-vis absorption spectra by transformation based on the Kubelka–Munk function versus the energy of light. The transformation was conducted according to the formula: $(\alpha h\nu)^2 = A(h\nu - E_g)$, where α , ν , A , and E_g are the absorption coefficient, light frequency, proportionality constant, and band gap, respectively [36]. As shown in Table 1, the band gaps of the doped samples were smaller than that of pristine SrTiO₃ and decreased with increasing g-C₃N₄ nanosheet dispersion during the preparation of the precursor to the doped samples. It is suggested that the g-C₃N₄ nanosheet can directly contribute to doping.

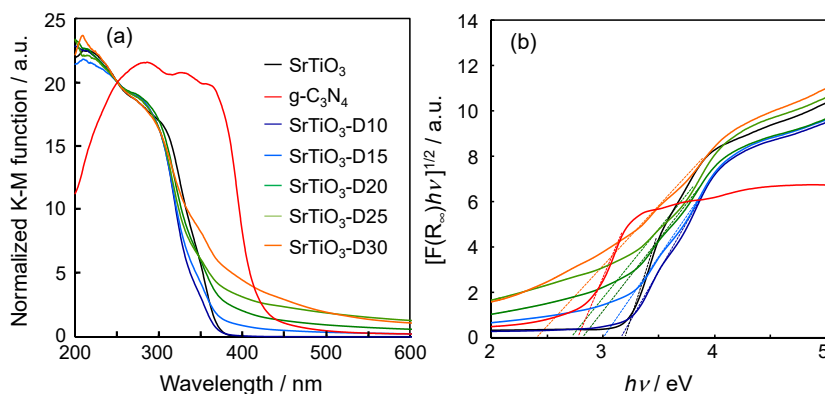


Figure 4. Diffuse reflectance UV-Vis absorption spectra (a) of SrTiO₃, C₃N₄, and the doped samples, and their Tauc plots (b).

Table 1. Band gap energy of the doped samples, SrTiO₃, and C₃N₄ nanosheet.

Sample	Band Gap/eV
SrTiO ₃	3.21
C ₃ N ₄ nanosheet	2.78
SrTiO ₃ -D10	3.17
SrTiO ₃ -D15	3.02
SrTiO ₃ -D20	2.81
SrTiO ₃ -D25	2.74
SrTiO ₃ -D30	2.42

3.2. The Photocatalytic Property of Doped SrTiO₃

At first, the photocatalytic activities of the doped samples were evaluated by considering the hydrogen evolution in the presence of methanol as a sacrificial agent. Figure 5 shows the hydrogen evolution rate for the doped samples synthesized using different amounts of g-C₃N₄ nanosheet dispersion. From the results of the UV-vis absorption analysis, it can be seen that the amount of dopant increased with increasing g-C₃N₄ nanosheet dispersion during the preparation of the precursor materials. The hydrogen evolution rate increased with increasing dopant concentration; however, excess increase of dopant makes the recombination center between the photogenerated electrons and holes increase [17]. SrTiO₃-D15 prepared using 15 mL C₃N₄ nanosheet dispersion, therefore, showed maximum photocatalytic activity. The hydrogen evolution rate of SrTiO₃-D15 was higher than those of pristine g-C₃N₄ and SrTiO₃ nanoparticles (Figure 6), suggesting that the photocatalytic activity of SrTiO₃-D15 increased due to a synergistic effect between SrTiO₃ and the dopant. To enhance the photocatalytic activity, Pt was loaded onto the SrTiO₃-D15 as a co-catalyst. The Pt loading sample showed photocatalytic activity under visible light irradiation ($\lambda > 420$ nm) (Figure S2). The 5-h photocatalytic test under UV irradiation using the Pt loaded sample could be repeated two times without noticeable deactivation (Figure S3). Figure 7 shows the effect of photocatalytic activity on Pt loading. The photocatalytic H₂ evolution rate showed maximum value at 0.2 wt% loading.

The photo-formed electron transfers to the Pt nanoparticle owing to a high work function, and proton reduction can efficiently take place over the Pt nanoparticles.

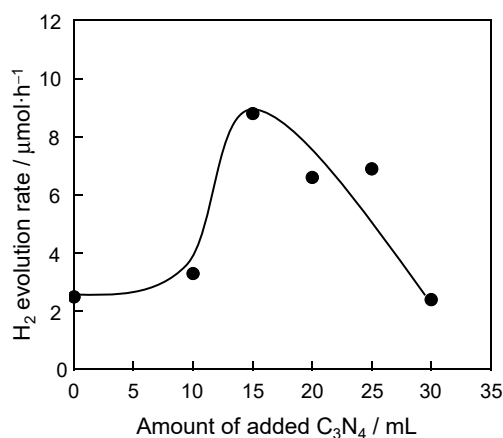


Figure 5. Photocatalytic H₂ evolution over the doped SrTiO₃ synthesized using different amounts of g-C₃N₄ nanosheet dispersion under UV light irradiation. The photocatalytic reaction was performed in an external-irradiation quartz cell under irradiation from a 500 W Xe lamp, 150 mL of a 50% methanol solution, and 0.1 g of a photocatalyst.

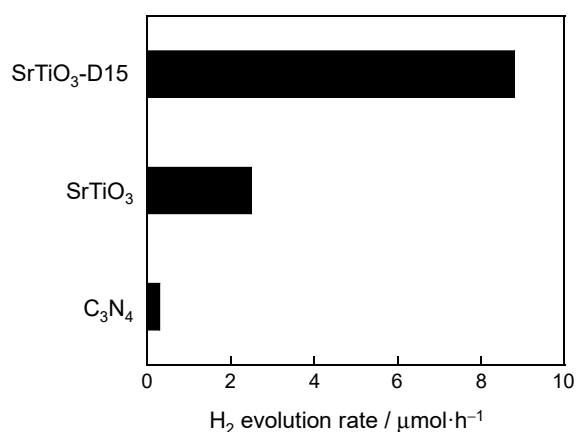


Figure 6. Comparison of photocatalytic activity under UV light irradiation between SrTiO₃-D15 and pristine SrTiO₃ and C₃N₄.

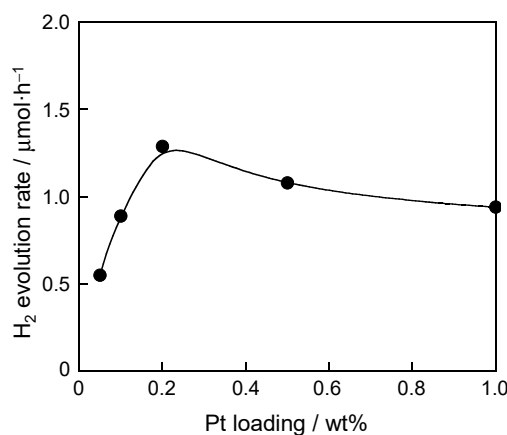


Figure 7. The effect of Pt loading on the photocatalytic H₂ evolution rate over SrTiO₃-D15 under visible light irradiation. The photocatalytic reaction was performed in an external-irradiation quartz cell under irradiation from a 500 W Xe lamp with a cut-off filter ($\lambda > 420$ nm), 150 mL of 50% methanol solution, and 0.1 g of photocatalyst.

4. Conclusions

We demonstrate a new doping method using g-C₃N₄ nanosheets. C₃N₄ nanosheets reacted with SrTiO₃ nanoparticles via a strong adsorption interaction to form the doped sample. The doped sample shows light absorption in a longer wavelength region ($\lambda > 420$ nm) compared to SrTiO₃. The photocatalytic activity of the doped sample under UV irradiation was higher than those of both pristine g-C₃N₄ and SrTiO₃ nanoparticles owing to their synergistic effect, and was enhanced by Pt loading. Moreover, the doped sample can operate under visible light irradiation. This doping method can be applied to a broad range of oxide-based photocatalysts. We investigated the photocatalytic properties of various doped samples prepared by this method. However, the photocatalytic H₂ evolution reaction in the doped sample cannot proceed without a sacrificial agent under visible light irradiation. Therefore, the overall water splitting under visible light irradiation should be investigated in the Z-scheme reaction system formed by combination with O₂ evolution photocatalysts.

Supplementary Materials: The following are available online at <http://www.mdpi.com/2571-6131/3/1/3/s1>, Figure S1: The photograph of samples, Figure S2: Time course of H₂ evolution reaction over 0.2 wt% Pt loaded SrTiO₃-D15, Figure S3: The repeated photocatalytic test, Table S1: The peak position and d-spacing in XRD of doped samples.

Author Contributions: Conceptualization, K.I.; Methodology, K.I.; Formal Analysis, Y.Y. and M.S.; Investigation, Y.Y.; Resources, K.I.; Writing—Original Draft Preparation, K.I.; Writing—Review & Editing, K.I.; Supervision, K.I. All authors have read and agreed to the published version of the manuscript.

Funding: This work was supported by the Regional Innovation Strategy Support Program 2014 of the Ministry of Education, Culture, Sports, Science and Technology, Japan (MEXT).

Acknowledgments: We thank Honmyo and Kawaguchi (Toda Kogyo Co. Ltd.) for supplying SrTiO₃ powder and some advice.

Conflicts of Interest: The authors declare no conflict of interest.

References

1. Kudo, A.; Miseki, Y. Heterogeneous photocatalyst materials for water splitting. *Chem. Soc. Rev.* **2008**, *38*, 253–278. [[CrossRef](#)] [[PubMed](#)]
2. Chen, X.; Shen, S.; Guo, L.; Mao, S.S. Semiconductor-based photocatalytic hydrogen generation. *Chem. Rev.* **2010**, *110*, 6503–6570. [[CrossRef](#)] [[PubMed](#)]
3. Hisatomi, T.; Kubo, J.; Domen, K. Recent advances in semiconductors for photocatalytic and photoelectrochemical water splitting. *Chem. Soc. Rev.* **2014**, *43*, 7520–7535. [[CrossRef](#)] [[PubMed](#)]
4. Osterloh, F.E. Inorganic materials as catalysts for photochemical splitting of water. *Chem. Mater.* **2008**, *20*, 35–54. [[CrossRef](#)]
5. Li, X.; Yu, J.; Low, J.; Fang, Y.; Xiao, J.; Chen, X. Engineering heterogeneous semiconductors for solar water splitting. *J. Mater. Chem. A* **2015**, *3*, 2485–2534. [[CrossRef](#)]
6. Abe, R. Recent progress on photocatalytic and photoelectrochemical water splitting under visible light irradiation. *J. Photochem. Photobiol. C Photochem. Rev.* **2010**, *11*, 179–209. [[CrossRef](#)]
7. Maeda, K. Photocatalytic water splitting using semiconductor particles: History and recent developments. *J. Photochem. Photobiol. C Photochem. Rev.* **2011**, *12*, 237–268. [[CrossRef](#)]
8. Maeda, K. Z-scheme water splitting using two different semiconductor photocatalysts. *ACS Catal.* **2013**, *3*, 1486–1503. [[CrossRef](#)]
9. Wang, Y.; Wang, X.; Antonietti, M. Polymeric graphitic carbon nitride as a heterogeneous organocatalyst: From photochemistry to multipurpose catalysis to sustainable chemistry. *Angew. Chem. Int. Ed.* **2012**, *51*, 68–89. [[CrossRef](#)]
10. Zhang, N.; Zhang, Y.; Xu, Y.-J. Recent progress on graphene-based photocatalysts: Current status and future perspectives. *Nanoscale* **2012**, *4*, 5792–5813. [[CrossRef](#)]
11. Fujishima, A.; Honda, K. Electrochemical photolysis of water at a semiconductor electrode. *Nature* **1972**, *238*, 37–38. [[CrossRef](#)] [[PubMed](#)]
12. Fujishima, A.; Zhang, X.; Tryk, D.A. TiO₂ photocatalysis and related surface phenomena. *Surf. Sci. Rep.* **2008**, *63*, 515–582. [[CrossRef](#)]

13. Ni, M.; Leung, M.K.H.; Leung, D.Y.C.; Sumathy, K. A review and recent developments in photocatalytic water-splitting using TiO₂ for hydrogen production. *Renew. Sustain. Energy Rev.* **2007**, *11*, 401–425. [[CrossRef](#)]
14. Leung, D.Y.C.; Fu, X.L.; Wang, C.F.; Ni, M.; Leung, M.K.H.; Wang, X.X.; Fu, X.Z. Hydrogen production over titania-based photocatalysts. *ChemSusChem* **2010**, *3*, 681–694. [[CrossRef](#)]
15. Qi, K.; Cheng, B.; Yu, J.; Ho, W. A review on TiO₂-based Z-scheme photocatalysts. *Chin. J. Catal.* **2017**, *38*, 1936–1955. [[CrossRef](#)]
16. Ishii, T.; Kato, H.; Kudo, A. H₂ evolution from an aqueous methanol solution on SrTiO₃ photocatalysts codoped with chromium and tantalum ions under visible light irradiation. *J. Photochem. Photobiol. A Chem.* **2004**, *163*, 181–186. [[CrossRef](#)]
17. Konta, R.; Ishii, T.; Kato, H.; Kudo, A. Photocatalytic activities of noble metal ion doped SrTiO₃ under visible light irradiation. *J. Phys. Chem. B* **2004**, *108*, 8992–8995. [[CrossRef](#)]
18. Ohno, T.; Mitsui, T.; Matsumura, M. Photocatalytic activity of S-doped TiO₂ photocatalyst under visible light. *Chem. Lett.* **2003**, *32*, 364–365. [[CrossRef](#)]
19. Asahi, R.; Morikawa, T.; Ohwaki, T.; Aoki, K.; Taga, Y. Visible-light photocatalysis in nitrogen-doped titanium oxides. *Science* **2001**, *293*, 269–271. [[CrossRef](#)]
20. Irie, H.; Watanabe, Y.; Hashimoto, K. Carbon-doped anatase TiO₂ powder as a visible-light sensitive photocatalyst. *Chem. Lett.* **2003**, *32*, 772–773. [[CrossRef](#)]
21. Maeda, K.; Domen, K. New non-oxide photocatalysts designed for overall water splitting under visible light. *J. Phys. Chem. C* **2007**, *111*, 7851–7861. [[CrossRef](#)]
22. Maeda, K.; Takata, T.; Hara, M.; Saito, N.; Inoue, Y.; Kobayashi, H.; Domen, K. GaN:ZnO solid solution as a photocatalyst for visible-light-driven overall water splitting. *J. Am. Chem. Soc.* **2005**, *127*, 8286–8287. [[CrossRef](#)]
23. Maeda, K.; Teramura, K.; Takata, T.; Hara, M.; Saito, N.; Toda, K.; Inoue, Y.; Kobayashi, H.; Domen, K. Overall water splitting on (Ga_{1-x}Zn_x)(N_{1-x}O_x) solid solution photocatalyst: Relationship between physical properties and photocatalytic activity. *J. Phys. Chem. B* **2005**, *109*, 20504–20510. [[CrossRef](#)] [[PubMed](#)]
24. Ong, W.-J.; Tan, L.-L.; Ng, Y.H.; Yong, S.-T.; Chai, S.-P. Graphitic carbon nitride (g-C₃N₄)-based photocatalysts for artificial photosynthesis and environmental remediation: Are we a step closer to achieving sustainability? *Chem. Rev.* **2016**, *116*, 7159–7329. [[CrossRef](#)]
25. Sun, S.; Sun, M.; Fang, Y.; Wang, Y.; Wang, H. One-step in situ calcination synthesis of g-C₃N₄/N-TiO₂ hybrids with enhanced photoactivity. *RSC Adv.* **2016**, *6*, 13063–13071. [[CrossRef](#)]
26. Liu, J.; Liu, Y.; Liu, N.; Han, Y.; Zhang, X.; Huang, H.; Lifshitz, Y.; Lee, S.-T.; Zhong, J.; Kang, Z. Metal-free efficient photocatalyst for stable visible water splitting via a two-electron pathway. *Science* **2015**, *347*, 970–974. [[CrossRef](#)]
27. Wang, X.; Maeda, K.; Chen, X.; Takanabe, K.; Domen, K.; Hou, Y.; Fu, X.; Antonietti, M. Polymer semiconductors for artificial photosynthesis: Hydrogen evolution by mesoporous graphitic carbon nitride with visible light. *J. Am. Chem. Soc.* **2009**, *131*, 1680–1681. [[CrossRef](#)]
28. Zhang, Y.; Liu, J.; Wu, G.; Chen, W. Porous graphitic carbon nitride synthesized via direct polymerization of urea for efficient sunlight-driven photocatalytic hydrogen production. *Nanoscale* **2012**, *4*, 5300–5303. [[CrossRef](#)]
29. Wang, X.C.; Maeda, K.; Thomas, A.; Takanabe, K.; Xin, G.; Carlsson, J.M.; Domen, K.; Antonietti, M. A metal-free polymeric photocatalyst for hydrogen production from water under visible light. *Nat. Mater.* **2009**, *8*, 76–82. [[CrossRef](#)]
30. Xu, X.; Liu, G.; Random, C.; Irvine, J.T.S. g-C₃N₄ coated SrTiO₃ as an efficient photocatalyst for H₂ production in aqueous solution under visible light irradiation. *Int. J. Hydrogen Energy* **2011**, *36*, 13501–13507. [[CrossRef](#)]
31. Li, J.; Zhang, M.; Li, Q.; Yang, J. Enhanced visible light activity on direct contact Z-scheme g-C₃N₄-TiO₂ photocatalyst. *Appl. Surf. Sci.* **2017**, *391*, 184–193. [[CrossRef](#)]
32. Chen, J.; Yang, Q.; Zhong, J.; Li, J.; Hu, C.; Deng, Z.; Duan, R. In-Situ construction of direct Z-scheme Bi₂WO₆/g-C₃N₄ composites with remarkably promoted solar-driven photocatalytic activity. *Mater. Chem. Phys.* **2018**, *217*, 207–215. [[CrossRef](#)]
33. Opoku, F.; Govender, K.K.; Sittert, C.G.C.E.; Govender, P.P. Insights into the photocatalytic mechanism of mediator-free direct Z-scheme g-C₃N₄/Bi₂MoO₆(010) and g-C₃N₄/Bi₂WO₆(010) heterostructures: A hybrid density functional theory study. *Appl. Surf. Sci.* **2018**, *427*, 487–498. [[CrossRef](#)]

34. Yang, Y.; Geng, L.; Guo, Y.; Meng, J.; Guo, Y. Easy dispersion and excellent visible-light photocatalytic activity of the ultrathin urea-derived g-C₃N₄ nanosheets. *Appl. Surf. Sci.* **2017**, *425*, 535–546. [[CrossRef](#)]
35. He, Y.M.; Wang, Y.; Zhang, L.H.; Teng, B.T.; Fan, M.H. High-efficiency conversion of CO₂ to fuel over ZnO/g-C₃N₄ photocatalyst. *Appl. Catal. B Environ.* **2015**, *168*, 1–8.
36. Sun, M.X.; Fang, Y.L.; Wang, Y.; Sun, S.F.; He, J.; Yan, Z. Synthesis of Cu₂O/graphene/rutile TiO₂ nanorod ternary composites with enhanced photocatalytic activity. *J. Alloys Compd.* **2015**, *650*, 520–527. [[CrossRef](#)]



© 2020 by the authors. Licensee MDPI, Basel, Switzerland. This article is an open access article distributed under the terms and conditions of the Creative Commons Attribution (CC BY) license (<http://creativecommons.org/licenses/by/4.0/>).